Photoinduced Charge Transfer Dynamics in $WO_3/BiVO_4$ Photoanodes Probed through Mid-IR Transient Absorption Spectroscopy

Ivan Grigioni,[†,Θ] Mohamed Abdellah,[§,‡,Θ] Annamaria Corti,[†] Maria Vittoria Dozzi,[†] Leif Hammarström,*[,§] and Elena Selli*[,†]

[†]Dipartimento di Chimica, Università degli Studi di Milano, Via Golgi 19, 20133 Milano, Italy

[§]Department of Chemistry - Ångström Laboratory, Uppsala University, Box 523, 75120 Uppsala, Sweden

[‡]Department of Chemistry, Qena Faculty of Science, South Valley University, 83523 Qena, Egypt

Supporting Information Placeholder

ABSTRACT: The dynamics of photopromoted electrons in $BiVO_4$, WO_3 and $WO_3/BiVO_4$ heterojunction electrodes has been directly probed by transient absorption (TA) mid-infrared (mid-IR) spectroscopy in the picosecond to microsecond time range. By comparing the dynamics recorded with the two individual oxides at 2050 cm^{-1} with that of the heterojunction system after excitation at different wavelengths, electron transfer processes between selectively excited $BiVO_4$ and WO_3 have been directly tracked for the first time. These results support the charge carrier interactions which were previously hypothesized by probing the $BiVO_4$ hole dynamics through TA spectroscopy in the visible range. Nanosecond mid-IR TA experiments confirmed that charge carrier separation occurs in $WO_3/BiVO_4$ electrodes under visible light excitation, persisting up to the microsecond timescale.

Harvesting energy from sunlight and producing solar fuels by photon-to-chemical energy conversion is a promising approach to fulfill the challenge of a sustainable energy economy. Along this line, one of the most attractive goals is the development of photoelectrochemical cells for water splitting.[1] Due to its ~ 2.4 eV relatively narrow band gap, bismuth vanadate ($BiVO_4$) has been intensively studied as photoanode material for oxygen evolution.[2–4] However, its main drawback is the significant recombination of photogenerated electron-hole pairs mainly due to its poor electrical conductivity, the slow hole transfer for water oxidation and surface recombination.[5–7] In the $WO_3/BiVO_4$ composite heterojunction, efficient electron-hole separation may occur due to the favorable type II band alignment between the two oxides, with the exploitation of both the good charge transport properties of WO_3 and the strong absorption of visible radiation by $BiVO_4$.[8–12]

The complex processes occurring in the $WO_3/BiVO_4$ heterojunction after band gap excitation have been investigated through transient absorption (TA) spectroscopy by probing the hole dynamics in $BiVO_4$ in the visible range,[9,13,14] on the basis of the results obtained for pure $BiVO_4$ in this spectral window.[9,13–17] Here, direct information on the charge carrier dynamics in the $WO_3/BiVO_4$ heterojunction is provided by tracking the photoexcited electrons on the picosecond to microsecond time scale through mid-infrared transient absorption (mid-IR TA) spectroscopy.[18,19] The crucial role of WO_3 in mediating the electron extraction from photoexcited $BiVO_4$ is highlighted, leading to efficient electron-hole separation in the $WO_3/BiVO_4$ heterojunction.

The dynamics of electrons in several semiconductors, such as TiO_2, ZnO, WO_3, Fe_2O_3 and CdSe, can be followed in the IR range.[20–25] Upon reduction, the oxides show a characteristic coloration due to optical transitions involving the excitation at wavelengths longer than their band gap of either free conduction band (CB) electrons,[26] or electrons from intraband gap trap sites to the CB edge.[27–29] Indeed, we verified that the photoreduction of WO_3 films immersed in ethanol as hole scavenger resulted in mid-IR spectral changes attributable to CB electrons (**Figure S1**).

Also for $BiVO_4$ we found that a new mid-IR absorption feature extending in the 4000-1400 cm^{-1} range appears upon chemical reduction (see **SI** for details). **Figure 1** shows the IR spectra recorded with a $BiVO_4$ film immediately after contact with an aqueous $NaBH_4$ solution and at different time during exposure to air up to the complete relaxation.

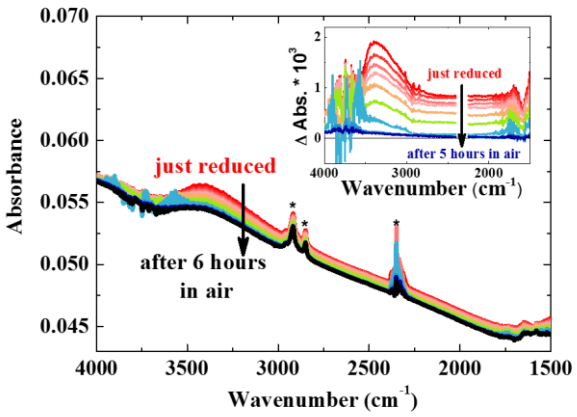

Figure 1. Spectral evolution in a $BiVO_4$ film exposed to air after reduction in aqueous $NaBH_4$. Asterisks indicate CO_2 absorption peaks. The red and the black traces were recorded right after $BiVO_4$ reduction and after 6 h-long exposure to air, respectively. Inset: difference absorption spectra during $BiVO_4$ re-oxidation.

The difference absorption spectra, obtained by subtracting the spectrum of the fully recovered film from the spectra recorded at different time during exposure to air (**Figure 1**, inset), show that the IR spectrum of reduced $BiVO_4$ uniformly relaxes in contact with air. This is confirmed by a comparison between the decay profiles recorded at 3350 and 2050 cm^{-1} (**Figure S2**). Reduced $BiVO_4$ reversibly undergoes oxidation in the presence of oxygen, while when it is stored under N_2 it retains its broad mid-IR absorption spectrum. Broad and featureless IR absorption, similar to that here observed in $BiVO_4$, is ascribed to free electrons.[18,30]

The procedures here employed for the preparation of WO_3, $BiVO_4$ and $WO_3/BiVO_4$ photoanodes and for the photoelectrochemical experiments are reported in the **SI**, together with their steady state UV-Vis absorption characterization (**Figure S3**). All WO_3 and $BiVO_4$ films on FTO were 410 and 45 nm thick, respectively. The photoelectrochemical responses of WO_3 and $BiVO_4$ electrodes are compared with that of the $WO_3/BiVO_4$ composite electrode in **Figure 2A**. With respect to the individual oxides, a significantly enhanced photocurrent is observed in the entire potential range for the composite electrode. This activity enhancement has been attributed to the favorable band alignment between the two oxides, which allows the injection of photopromoted electrons from the $BiVO_4$ CB to the WO_3 CB, where they can exploit the better charge mobility of the latter material.[8,9]

Furthermore, the incident photon to current efficiency (IPCE) measured with the $WO_3/BiVO_4$ coupled system outperforms the sum of the IPCE curves measured with the two individual oxides (see **Figure S4**) at wavelengths longer than the WO_3 absorption onset (ca. 460 nm). In contrast, for wavelengths shorter than 400 nm, the IPCE of the heterojunction system falls below the sum of the IPCE curves measured with the two individual semiconductors. Previous fs-TA measurements in the visible region to track $BiVO_4$ hole dynamics[14] indicate that charge recombination of electrons photopromoted in WO_3 with $BiVO_4$ holes may occur upon simultaneous $BiVO_4$ and WO_3 excitation.

Direct evidence of photoinduced charge transfer occurring in the $WO_3/BiVO_4$ heterojunction is here obtained by directly probing electrons in WO_3, $BiVO_4$ and $WO_3/BiVO_4$ films through IR-TA spectroscopy. The dynamics of photopromoted electrons in $BiVO_4$ after visible excitation was followed by TA in the 2300-1700 cm^{-1} range (**Figure S5**). These time-resolved spectra show an essentially flat induced absorption, similar to the steady-state IR spectra of chemically reduced $BiVO_4$ (**Figure 1**).

The mid-IR transient signal of $BiVO_4$ (**Figure 2B**) decays within few hundreds of picoseconds and shows a faster dynamics than the holes signal previously monitored in the visible,[9] which exhibits a ΔA tail extending longer than the fs-TA time window. This discrepancy was recently observed with pure $BiVO_4$ powders and ascribed to the free electrons fast relaxation to states not observable in the mid-IR region.[31] On the other hand, in WO_3 and in the $WO_3/BiVO_4$ coupled system, the 2050 cm^{-1} TA signal exhibits a relatively slower decay (**Figure 2B**). Quantitative information on the dynamics involved in $BiVO_4$ and in the other two systems was obtained by fitting the decay traces with a bi- and a tri-exponential equation (eq. S2 and S3), respectively. The resulting parameters are reported in **Table 1**.

Upon excitation at 410 nm, most of the electrons photopromoted in $BiVO_4$ alone decay with a time constant τ_1 of ~ 10 ps, while the remaining free electrons decay with a ca. 170 ps τ_2 time constant. Thus the TA signal disappears within the temporal window of our experiments, in line with the results of recent studies.[31] Power dependence measurements carried out on $BiVO_4$ (**Figure S6** and **SI**) indicate that the initial part (< 10 ps) of the mid-IR signal decay becomes progressively faster with increasing pump power at 410 nm. This corroborates the hypothesis that the ultrafast decay exhibited by the mid-IR TA signal in $BiVO_4$ can be mainly ascribed to trapping and cooling of free electrons into IR unobservable states, not to electron-hole recombination. In fact, the longer lasting relaxation of trapped holes was found to be independent of the pump power.[14] Charge recombination cannot be excluded and may be active during the first tenths of picoseconds, as for Fe_2O_3.[32]

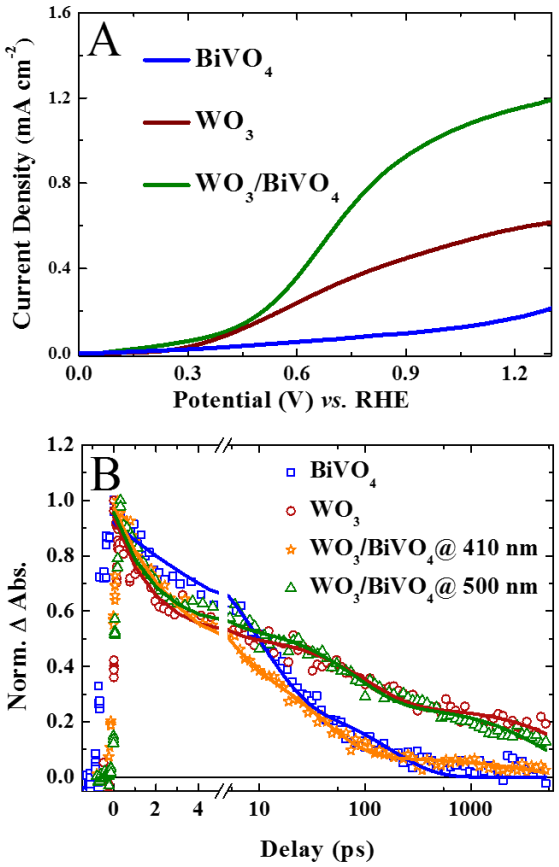

Figure 2. (A) Photocurrent density recorded in linear sweep voltammetry under simulated solar light with the WO_3 (brown), $BiVO_4$ (blue) and $WO_3/BiVO_4$ (green) electrodes in contact with 0.5 M Na_2SO_4. (B) IR-fs TA traces recorded at 2050 cm^{-1} with the WO_3 (red circles), $BiVO_4$ (blue squares) and $WO_3/BiVO_4$ (orange stars) electrodes upon 410 nm excitation (270 nJ/pulse) and with $WO_3/BiVO_4$ upon 500 nm excitation (300 nJ/pulse; green triangles).

Table 1. Fitting parameters of the decay traces obtained with the investigated materials upon excitation at 410 nm or 500 nm.

	WO_3 410 nm	$BiVO_4$ 410 nm	$WO_3/BiVO_4$ 410 nm	$WO_3/BiVO_4$ 500 nm
A_1 (%)	45±2	70±4	54±2	42±1
τ_1 (ps)	1.9±0.2	10.0±0.8	3.1±0.2	1.89±0.15
A_2 (%)	28±2	30±9	39±2	31±1
τ_2 (ps)	105±15	171±26	39±3	81±8
A_3 (%)	27±2		7±1	27±1
τ_3 (ns)	11±3		3.4±0.9	5.3±0.6
Red. χ^2	1.0 10^{-3}	1.3 10^{-3}	3.5 10^{-4}	6.0 10^{-4}

As shown in **Table 1**, in the case of the WO_3 and $WO_3/BiVO_4$ electrodes, even if almost 50% of the photogenerated signal de-

cays within ~ 2 ps, a longer time constant τ_3 is required to fit their decay profile. This suggests the presence of long-lived electrons, persisting also beyond the time scale of our fs-TA experiments.

The fastest decay component found in WO_3 may be ascribed either to its free carriers intrinsically living shorter than in other oxides, for example TiO_2 and $BiVO_4$,[21,31] or to power dependent second order electron-hole recombination.[33] Remarkably, the τ_1 time constant found in the $WO_3/BiVO_4$ system upon 500 nm excitation is equal to that observed in WO_3 and smaller with respect to those obtained in $BiVO_4$ upon 410 and 500 nm excitation. This suggests that the electron transfer between $BiVO_4$ photoexcited at 500 nm and WO_3 is faster than the response function of our experimental set-up (~200 fs). Moreover, the τ_1 value found for the coupled system upon 410 nm excitation is intermediate between the τ_1 values obtained for the two separate oxides upon 410 nm excitation. This can be explained considering that the WO_3 CB gets partially filled under 410 nm excitation and thus electron injection from excited $BiVO_4$ CB may be partly hindered by coulombic repulsion.

The second component, τ_2, is much shorter in $WO_3/BiVO_4$ than in either WO_3 or $BiVO_4$. Under 410 nm pump, both oxides are excited and the shorter τ_2 value obtained for the coupled system with respect to $BiVO_4$ is in line with the hypothesis that a recombination process opens between electrons photopromoted in WO_3 and $BiVO_4$ valence band (VB) holes.[14] The effect of 410 nm vs. 500 nm excitation is even more apparent on τ_3. Selective excitation of $BiVO_4$ with the 500 nm pump in the $WO_3/BiVO_4$ heterojunction electrode leads to a striking increase of the lifetime of photopromoted electrons. Indeed τ_2 and τ_3 show a two-fold increase, while the A_3 weighing coefficient is almost four time larger, with respect to 410 nm excitation (see **Table 1** and the green and orange traces in **Figure 2B**), with time constant values closely matching those obtained with WO_3 (red trace in **Figure 2B**). On the other hand, the IR signal decay found by exciting individual $BiVO_4$ at 500 nm was even faster than under 410 nm excitation (**Figure S7**). This excludes the hypothesis that the slower mid-IR signal decay observed upon exciting $WO_3/BiVO_4$ at 500 nm instead of at 410 nm is merely due to an excitation wavelength dependent charge dynamics in $BiVO_4$.

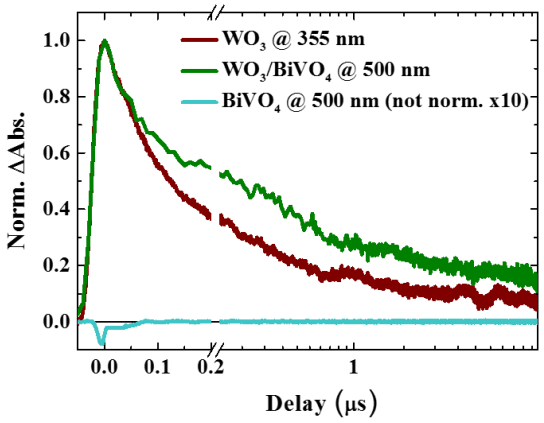

Figure 3. Infrared nanosecond TA traces recorded at 2050 cm^{-1} with neat WO_3 upon 355 nm excitation (brown), and with the $WO_3/BiVO_4$ composite (green) and neat $BiVO_4$ (light blue) upon 500 nm excitation.

The lifetime increase of trapped electrons in $WO_3/BiVO_4$ upon 500 nm excitation parallels that previously observed for trapped holes in the same coupled system (**Figure S8**). This confirms the key role played by WO_3 in increasing the lifetime of both photogenerated charge carriers. Consequently, the electron lifetime in the $WO_3/BiVO_4$ electrode excited at 500 nm is expected to extend beyond our fs TA window (~ 5 ns). Therefore, flash photolysis experiments up to the microsecond time scale, with a 2050 cm^{-1} probe, were performed to measure the actual lifetimes of the photopromoted electrons (**Figure 3**).

Since free electrons photopromoted in $BiVO_4$ decay within 1 ns, the absorption observed in flash photolysis experiments is generated exclusively by longer living electrons in WO_3. Indeed, WO_3 containing electrodes clearly show a long-lived IR signal (**Figure 3**). Also selective excitation of $BiVO_4$ at 500 nm in $WO_3/BiVO_4$ generates a long-lived IR signal, which provides uncontroversial evidence that electrons photopromoted in $BiVO_4$ CB promptly move to the WO_3 CB. Thus, very long-lived electrons in the heterojunction film are photoproduced under visible light excitation, and are here detected for the first time by mid-IR spectroscopy.

Scheme 1. The excitation wavelength dependent electronic interactions in $WO_3/BiVO_4$ under (A) selective excitation of $BiVO_4$ and (B) simultaneous excitation of both oxides (500 and 410 nm pump, respectively).

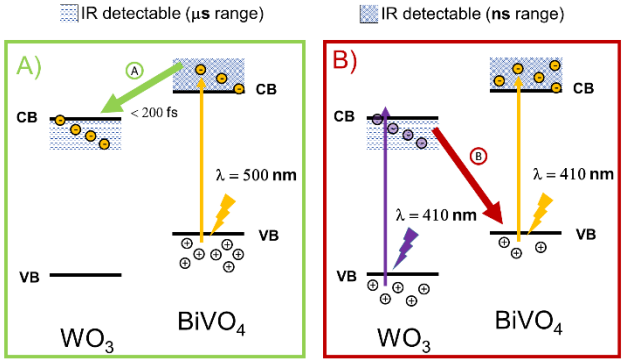

In conclusion, photopromoted electrons live much longer in WO_3 than in $BiVO_4$, in line with the far better electron conductivity of the former oxide. The main electron transfer pathways occurring between the two oxides in the heterojunction system are illustrated in **Scheme 1**. Free electrons photoexcited under visible light in the $BiVO_4$ CB can avoid trapping and recombination in $BiVO_4$ by flowing into WO_3 where they live longer (path A in **Scheme 1A**). Thus WO_3 has a key role in elongating the electron lifetime in the $WO_3/BiVO_4$ heterojunction under visible light excitation. On the other hand, a recombination channel between electrons photopromoted in WO_3 and holes in the $BiVO_4$ VB is active upon simultaneous excitation of both oxides (path B in **Scheme 1B**). Therefore, in optimized heterojunctions, care should be taken to avoid this parasitic process.

▪ ASSOCIATED CONTENT

Supporting Information

The Supporting Information is available free of charge on the ACS Publications website. Experimental section; IR spectra of reduced WO_3 and $BiVO_4$; steady-state UV-Vis absorption spectra, IPCE measurements; complementary time-resolved IR experiments and data; power and wavelength dependent excitation of $BiVO_4$; hole vs. electron TA dynamics (PDF).

▪ AUTHOR INFORMATION

Corresponding Author
Prof. Leif Hammarström (*) leif.hammarstrom@kemi.uu.se
Prof. Elena Selli (*) elena.selli@unimi.it

Author Contributions
[Θ] These authors contributed equally.

ORCID

Ivan Grigioni: 0000-0002-9469-4570
Mohamed Abdellah: 0000-0002-6875-5886
Maria Vittoria Dozzi: 0000-0002-6390-9348
Elena Selli: 0000-0001-8391-7639
Leif Hammarström: 0000-0002-9933-9084

Notes
The authors declare no competing financial interests.

ACKNOWLEDGMENTS

This work originates from an Erasmus master student exchange. IG, MVD and ES gratefully acknowledge financial support from Fondazione Cariplo 2013-0615 and MIUR PRIN 2015K7FZLH projects. The use of instrumentation purchased through the SmartMatLab project, Fondazione Cariplo grant 2013-1766, is gratefully acknowledged. IG thanks Fondazione Fratelli Confalonieri for a supporting grant. LH and MA gratefully acknowledge financial support from the Knut and Alice Wallenberg Foundation (2011:0067) and the Foundation Olle Engkvist Byggmästare (2016/3)

▪ REFERENCES

(1) Armstrong, R. C.; Wolfram, C. D.; de Jong, K. P.; Gross, R.; Lewis, N. S.; Boardman, B.; Ragauskas, A. J.; Ehrhardt-Martinez, K.; Crabtree, G.; Ramana, M. V. *Nat. Energy* **2016**, *1*, 15020.
(2) Park, Y.; McDonald, K. J.; Choi, K.-S. *Chem. Soc. Rev.* **2013**, *42*, 2321.
(3) Kim, T. W.; Choi, K.-S. *Science.* **2014**, *343*, 990.
(4) Kim, J. H.; Jang, J.-W.; Jo, Y. H.; Abdi, F. F.; Lee, Y. H.; van de Krol, R.; Lee, J. S. *Nat. Commun.* **2016**, *7*, 13380.
(5) Zhong, D. K.; Choi, S.; Gamelin, D. R. *J. Am. Chem. Soc.* **2011**, *133*, 18370.
(6) Abdi, F. F.; Savenije, T. J.; May, M. M.; Dam, B.; Van De Krol, R. *J. Phys. Chem. Lett.* **2013**, *4*, 2752.
(7) Zachäus, C.; Abdi, F. F.; Peter, L. M.; Van De Krol, R. *Chem. Sci.* **2017**, *8*, 3712.
(8) Hong, S. J.; Lee, S.; Jang, J. S.; Lee, J. S. *Energy Environ. Sci.* **2011**, *4*, 1781.
(9) Grigioni, I.; Stamplecoskie, K. G.; Selli, E.; Kamat, P. V. *J. Phys. Chem. C* **2015**, *119*, 20792.
(10) Shi, X.; Herraiz-Cardona, I.; Bertoluzzi, L.; Lopez-Varo, P.; Bisquert, J.; Giménez, S. *Phys. Chem. Chem. Phys.* **2016**, *18*, 9255.
(11) Chae, S. Y.; Lee, C. S.; Jung, H.; Joo, O.-S.; Min, B. K.; Kim, J. H.; Hwang, Y. J. *ACS Appl. Mater. Interfaces* **2017**, *9*, 19780.
(12) Van, C. N.; Do, T. H.; Chen, J. W.; Tzeng, W. Y.; Tsai, K. A.; Song, H.; Liu, H. J.; Lin, Y. C.; Chen, Y. C.; Wu, C. L.; Luo, C. W.; Chou, W. C.; Huang, R.; Hsu, Y. J.; Chu, Y. H. *NPG Asia Mater.* **2017**, *9*, e357.
(13) Loiudice, A.; Cooper, J. K.; Hess, L. H.; Mattox, T. M.; Sharp, I. D.; Buonsanti, R. *Nano Lett.* **2015**, *15*, 7347.
(14) Grigioni, I.; Stamplecoskie, K. G.; Jara, D. H.; Dozzi, M. V.; Oriana, A.; Cerullo, G.; Kamat, P. V.; Selli, E. *ACS Energy Lett.* **2017**, *2*, 1362.
(15) Aiga, N.; Jia, Q.; Watanabe, K.; Kudo, A.; Sugimoto, T.; Matsumoto, Y. *J. Phys. Chem. C* **2013**, *117*, 9881.
(16) Ravensbergen, J.; Abdi, F. F.; Van Santen, J. H.; Frese, R. N.; Dam, B.; Van De Krol, R.; Kennis, J. T. M. *J. Phys. Chem. C* **2014**, *118*, 27793.
(17) Ma, Y.; Pendlebury, S. R.; Reynal, A.; Formal, L.; James, R.; Le Formal, F.; Durrant, J. R. *Chem. Sci.* **2014**, *5*, 2964.
(18) Yoshihara, T.; Katoh, R.; Furube, A.; Tamaki, Y.; Murai, M.; Hara, K.; Murata, S.; Arakawa, H.; Tachiya, M. *J. Phys. Chem. B* **2004**, *108*, 3817.
(19) Tamaki, Y.; Hara, K.; Katoh, R.; Tachiya, M.; Furube, A. *J. Phys. Chem. C* **2009**, *113*, 11741.
(20) Kolle, U.; Moser, J. E.; Grätzel, M. *Inorg. Chem.* **1984**, *24*, 2253.
(21) Antila, L. J.; Santomauro, F. G.; Hammarström, L.; Fernandes, D. L. A.; Sá, J. *Chem. Commun.* **2015**, *51*, 10914.
(22) Cieślak, A. M.; Pavliuk, M. V.; D'Amario, L.; Abdellah, M.; Sokołowski, K.; Rybinska, U.; Fernandes, D. L. A.; Leszczyński, M. K.; Mamedov, F.; El-Zhory, A. M.; Föhlinger, J.; Budinská, A.; Wolska-Pietkiewicz, M.; Hammarström, L.; Lewiński, J.; Sá, J. *Nano Energy* **2016**, *30*, 187.
(23) Abdellah, M.; El-Zohry, A. M.; Antila, L. J.; Windle, C. D.; Reisner, E.; Hammarström, L. *J. Am. Chem. Soc.* **2017**, *139*, 1226.
(24) Huang, Z.; Lin, Y.; Xiang, X.; Rodriguez-Cordoba, W.; McDonald, K. J.; Hagen, K. S.; Choi, K.; Brunschwig, B. S.; Musaev, D. G.; Hill, C. L.; Wang, D.; Lian, T. *Energy Environ. Sci.* **2012**, *5*, 8923.
(25) Klimov, V.; McBranch, D.; Leatherdale, C.; Bawendi, M. *Phys. Rev. B* **1999**, *60*, 13740.
(26) Wang, C.; Wang, C.; Shim, M.; Shim, M.; Guyot-sionnest, P. *Science* **2001**, *291*, 2390.
(27) Di Valentin, C.; Pacchioni, G.; Selloni, A. *J. Phys. Chem. C* **2009**, *113*, 20543.
(28) Yamase, T. *Chem. Rev.* **1998**, *2665*, 307.
(29) Bedja, I.; Hotchandani, S.; Kamat, P. V. *J. Phys. Chem.* **1993**, *97*, 11064.
(30) Pankove, I. J. *Opt. Process. Semicond.* **1971**, Dover: New York.
(31) Suzuki, Y.; Murthy, D. H. K.; Matsuzaki, H.; Furube, A.; Wang, Q.; Hisatomi, T.; Domen, K.; Seki, K. *J. Phys. Chem. C* **2017**, *121*, 19044.
(32) Huang, Z.; Lin, Y.; Xiang, X.; Rodríguez-Córdoba, W.; McDonald, K. J.; Hagen, K. S.; Choi, K.-S.; Brunschwig, B. S.; Musaev, D. G.; Hill, C. L.; Wang, D.; Lian, T. *Energy Environ. Sci.* **2012**, *5*, 8923.
(33) Matsuzaki, H.; Matsui, Y.; Uchida, R.; Yada, H.; Terashige, T.; Li, B.-S.; Sawa, A.; Kawasaki, M.; Tokura, Y.; Okamoto, H. *J. Appl. Electrochem.* **2014**, *053514*.